Supporting Information

Alkaline Electrocatalytic Water Oxidation by Fe-Ni Nanostructures on Porous Turbostratic Carbon with Tailorable Metal-Metal Active Sites

Dipankar Saha[1], Chaoyun Tang[2], Javed Khan[2], Pulkit Jain[2], Cheng-Jie Yang[3], Chung-Li Dong[3], Richard F. Webster,[4] Chi-Liang Chen[5], Zhu Chen[2], Peng Bai[2], Richard M. Tilley[4,6], Nianqiang Wu[2*], and James J. Watkins[1]*

[1]Conte Center for Polymer Research, Department of Polymer Science and Engineering, University of Massachusetts, Amherst, Massachusetts 01003, United States.
[2]Department of Chemical and Biomolecular Engineering, University of Massachusetts, Amherst, Massachusetts 01003, United States.
[3]Department of Physics, Tamkang University, Tamsui 25137, Taiwan
[4]Mark Wainwright Analytical Centre, The University of New South Wales, Sydney, NSW 2052, Australia.
[5]National Synchrotron Radiation Research Center, Hsinchu 30076, Taiwan
[6]School of Chemistry, The University of New South Wales, Sydney, NSW 2052, Australia.

*Corresponding authors

nianqiangwu@umass.edu

watkins@polysci.umass.edu

MATERIALS AND METHODS

Chemicals and Materials

Unless otherwise noted, all materials were used without further purification. cis-5-Norbornene-exo-2,3-dicarboxylic anhydride, N,N′-didcyclohexylcarbodiimide (DCC, >99%), 4-dimethylaminopyridine (DMAP, >99%), 5-norbornene-2-endo,3-exodicarboxylic acid (97%), ethyl vinyl ether (>99%), dopamine hydrochloride, iron(II) chloride tetrahydrate (∼99%), nickel (II) nitrate hexahydrate (∼99%), magnesium sulfate (∼99.5%), ammonia solution (28–30%), anhydrous dimethylformamide (DMF, ∼99.8%), anhydrous dichloromethane (DCM, ∼99.8%), concentrated sulfuric acid (∼98%), and tetrahydrofuran (∼98%) were purchased from Sigma-Aldrich. Polymer Source provided the poly(ethylene glycol) monomethyl ether poly(styrene) (∼99%, Mw = 5 kg mol^{-1}) with a hydroxyl group and poly(styrene)-b-poly(ethylene oxide). Anhydrous ethanol was supplied from Fisher Scientific. Third-generation Grubb's catalyst (G3) was prepared based on the reported procedure. Silicon wafers were purchased from University Wafer, Inc. (Boston, MA, USA). Ultrapure type I water (18.2 MΩ·cm) was used for all the experiments.

Synthesis of Polystyrene-block-Poly(ethylene oxide) Bottlebrush Block Copolymers (PS-b-PEO BBCPs)

Symmetric poly[norbornene-graft-poly(styrene)]-block-[poly(norbornene-graft-poly(ethylene oxide)] (PS-*b*-PEO) BBCPs were synthesized according to previous work. In a typical polymerization, 50 mg of norbornene-functionalized PS (5 kDa) and 50 mg of norbornene-functionalized PEO (5 kDa) were transferred to an argon-filled glovebox. First, the PS and PEO macromonomer were dissolved separately in 1 mL of anhydrous DCM. Afterward, a stock solution of third-generation Grubbs catalyst (G3) (0.5 mg/mL) was prepared, and the appropriate amount was added to the PS solution for the desired molecular weight. After polymerization proceeded for

30 minutes, the PEO solution was transferred into the reaction flask and allowed to react for one hour. The reaction was terminated via the addition of 0.5 mL of ethyl vinyl ether. The reaction mixture was diluted, and an excess amount of thiol-functionalized silica gel (SiliaMets® Thiol) was added to scavenge G3. Following filtration through a 0.2 μm syringe filter, the solution was allowed to evaporate to air.

Preparation of Mesoporous Iron-Nickel Bottlebrush Block Copolymer Precursors

Dopamine (200 mg) and iron and nickel salts (according to the desired weight percentage) were dissolved in a mixture of ethanol and deionized water (4:1 volume ratio, total volume 8 mL). This dopamine solution was then added to 1 mL of THF containing 20 mg of PS-*b*-PEO, followed by vigorous vortex mixing for 2 minutes and continued stirring at 900 rpm for 1 hour. Afterward, polymerization of dopamine was initiated by the addition of 500 μL of an ammonia-aqueous solution (28-30%), causing the solution to turn dark brown or sometimes black. The reaction vessel was sealed with a punctured parafilm and allowed to react for 48 hours. After the reaction, the mixture was centrifuged at 7000 rpm and rinsed at least five times with a mixed solution. The resulting composite was collected as a precipitate, spread over a silicon wafer, and dried overnight under ambient conditions.

Photothermal Pyrolysis to Prepare Hierarchical Fe-Ni Nanostructures

Photothermal pyrolysis was conducted using a Novacentric Pulse Forge 1300 xenon flash lamp system (Austin, Texas) under ambient conditions. The samples were placed 10 mm from the lamp for treatment. Each sample, mounted on a silicon wafer, was exposed to 15 pulses at 400 V, with a pulse duration of 500 μs and a frequency of 1 Hz to ensure complete conversion of the polymer into porous turbostratic carbons. The yield of the processed sample was found to be 50%, based on the mass difference before and after photothermal treatment.

STEM-XEDS and STEM-EELS Methods and Analysis

The samples for aberration-corrected scanning transmission electron microscopy (AC-STEM) were prepared by drop-casting 5 μL of the sample dispersed in ethanol onto a copper (Cu) transmission electron microscopy (TEM) grid with a lacey carbon support film (Pacific Grid-Tech Cu-400LC). AC-STEM imaging, X-ray energy-dispersive spectroscopy (XEDS), and electron energy loss spectroscopy (EELS) were performed using a JEOL GrandARM300F2 microscope operated at 300 kV with a 24 mrad convergence angle. The collection semi-angles for the high-angle annular dark-field (HAADF) detector ranged from 79 to 180 mrad, while the bright-field (BF) STEM detector had an outer collection semi-angle of 10 mrad. The instrument was equipped with dual 158 mm^2 silicon drift X-ray detectors for EDS measurements. For EELS mapping, a Gatan Continuum (model 1069) spectrometer paired with a Gatan K3 direct electron camera was used. The EELS mapping employed the 5mm entrance aperture, which has a collection semi-angle of 72 mrad. Spectra were acquired at a dispersion of 0.18 eV/channel. Annular dark-field (ADF) images taken alongside the EELS data were collected using the Gatan ADF detector (model 807), with inner collection semi-angle of approximately 50 mrad. The energy resolution, defined by the full width at half maximum (FWHM) of the zero-loss peak (ZLP), was measured to be 0.405 eV. Images and spectra were processed using standard routines in Gatan Digital Micrograph. The TFS Spectra Ultra, featuring an ultra-high-resolution, double-corrected HRTEM/STEM, was operated at 300 kV to acquire HAADF-STEM images and XEDS maps.

Diffraction and Spectroscopy

X-ray diffraction (XRD) measurements were carried out using a Panalytical X-ray diffractometer equipped with Cu Kα radiation (wavelength = 1.5418 Å). XPS experiments were performed using a Physical Electronics VersaProbe III instrument equipped with a monochromatic Al kα x-ray source (hν = 1,486.6 eV) and a concentric hemispherical analyzer. Charge neutralization was performed using both low energy electrons (<5 eV) and argon ions. The binding energy axis was calibrated using sputter cleaned Cu (Cu $2p_{3/2}$ = 932.6 eV, Cu $3p_{3/2}$ = 75.1 eV) and Au foils (Au $4f_{7/2}$ = 83.9 eV). Peaks were charge referenced to CC-sp^2 peak of the carbon 1s spectra at 284.5 eV. Measurements were made at a takeoff angle of 45° with respect to the sample surface plane. This resulted in a typical sampling depth of 3-6 nm (95% of the signal originated from this depth or shallower). Quantification was done using instrumental relative sensitivity factors (RSFs) that account for the x-ray cross section and inelastic mean free path of the electrons. The analysis size was ~200μm in diameter. CasaXPS software was used to analyze the spectra. *Ex situ* Raman spectroscopy was performed using a DXR Raman microscope from Thermo Fisher Scientific. The spectral range covered 100-3500 cm^{-1} with a resolution of 5.3-8.8 cm^{-1}, utilizing a 20× objective and a backscattering geometry. To minimize damage to the samples, measurements were conducted with a 633 nm laser (power = 5 mW) focused on a spot size of 1.6 μm. Raman spectra were collected from three different spots on each sample.

Electrochemical Measurements and Electrode Preparation

All electrochemical measurements for the OER were conducted using a three-electrode setup in 1 M KOH at ambient temperature on a CH Instruments CHI660D electrochemical workstation. The working electrode was a glassy carbon electrode (GCE) modified with a Fe-Ni catalyst, the counter electrode was a graphite rod, and the reference electrode was an Ag/AgCl electrode in saturated KCl. To prepare the catalyst ink, 3 mg of the Fe-Ni catalyst was mixed with 8% Nafion, 20%

ethanol, and 80% water, then sonicated using a Qsonica probe sonicator for 15 minutes at room temperature. A 5 μL aliquot of this ink was drop-cast onto the GCE (with an active working area of 3 mm) to achieve a catalyst loading of 1 mg/cm², and then dried to form the working electrode. Linear sweep voltammetry (LSV) was conducted at a scan rate of 5 mV/s using the three-electrode system in 1 M KOH. All potentials reported are referenced to the reversible hydrogen electrode (RHE), with the equilibrium potential for OER set at 1.23 V vs. RHE. The overpotential is calculated as the difference between the measured potential and 1.23 V. Each electrochemical experiment was repeated at least three times to ensure reproducibility.

Turnover Frequency Calculations

TOF values of different electrodes were calculated based on the following equation.[1]

$$TOF = (J \times A)/ (4 \times F \times n)$$

Here, J (mA/cm^2) denotes the current density at the applied overpotential for the OER, A represents the geometric surface area of the electrode, F is the Faraday constant (96,485 C mol^{-1}), and n corresponds to the molar number of active sites on the electrode.

***In situ* Raman Measurements**

A custom-made cell with a three-electrode configuration was used to carry out in-situ Raman spectroscopy. Confocal Raman microscope (LABRAM HR Evolution, Horiba Instruments Inc.) was used in an epi-illumination configuration, with a 633 nm laser as the excitation source. The scattered Raman light was collected using a water immersion lens (Olympus, 40x, NA, 0.8), which was covered by a fluorinated ethylene propylene (FEP) film to prevent lens damage. The electrochemical measurements were performed by either Squidstat Plus potentiostat (Admiral Instruments) or Biologic SP 50e potentiostat (Biologic USA) in potentiostatic mode. The three-electrode setup consisted of GCE coated with catalyst as a working electrode, Ag/AgCl (CHI111,

CH Instruments Inc) as reference electrode, and platinum wire as (Alfa Aesar, 0.25 mm, 99.9% metal basis) counter electrode. The electrolyte used was 1M KOH (Fisher Scientific, >85%).

Preparation of MEA and performance Evaluation

The membrane electrode assembly (MEA) cell was directly purchased from Gaoshi Union Co., Ltd. Cathode membrane was purchased from Dioxide Materials (Commercial cathode for water electrolyzer). For the anode, homogeneous catalyst ink was prepared first. In a typical process, 8 mg of as-synthesized catalyst, 480 μL of 5 wt. % Nafion/Ethanol solution and 280 μL ethanol were mixed and sonicated for 20 mins. The ink was subsequently loaded onto GDL (Sigracet 22 BB, Fuel Cell Store, area: 2 × 2 cm^2) by hand-spraying. The GDL was fixed on a heated metal plate and kept at 120 ºC. As a result, the catalyst loading was 2 $mg \cdot cm^{-2}$, and the Nafion/catalyst ratio was 25 wt.%. The anion exchange membrane (AEM, Sustainion X37-50 Grade T, Dioxide Materials) was immersed in 1 M KOH for 2 h and then rinsed with fresh 1 M KOH to convert the acetate anion into hydroxide anion. Subsequently, the cathode and anode were sandwiched with the AEM and pressed to prepare an MEA device. 1 M KOH solution was used as an electrolyte, and the temperature of the electrolyte was controlled from room temperature to 80 °C by a constant temperature heating chamber. The potential range is from 1.3 to 2.3 V at a scan rate of 5 $mV \cdot s^{-1}$. The electrolyte was fed with a flow rate of 20 $mL \cdot min^{-1}$ by two peristaltic pumps (YZ1515x, LongerPump).

First-Principles Calculations

Spin-polarized, periodic DFT calculations were performed with the VASP software package, version 6.3.2, [2, 3] using the PBE exchange-correlation functional and the PAW method for treating core electrons. A plane-wave basis set with a kinetic energy cutoff of 400 eV was used for the valence electrons. A K-point grid with a mesh size of 2 x 2 x 1 was used for sampling of reciprocal

space. To calculate entropy using the harmonic oscillator approximation, vibrational frequency analysis was performed using central finite differences with a step size of 0.015 Å. The electronic self-consistency loop and structural optimization were converged to 10^{-6} eV and a force threshold of 0.02 eV/Å, respectively.

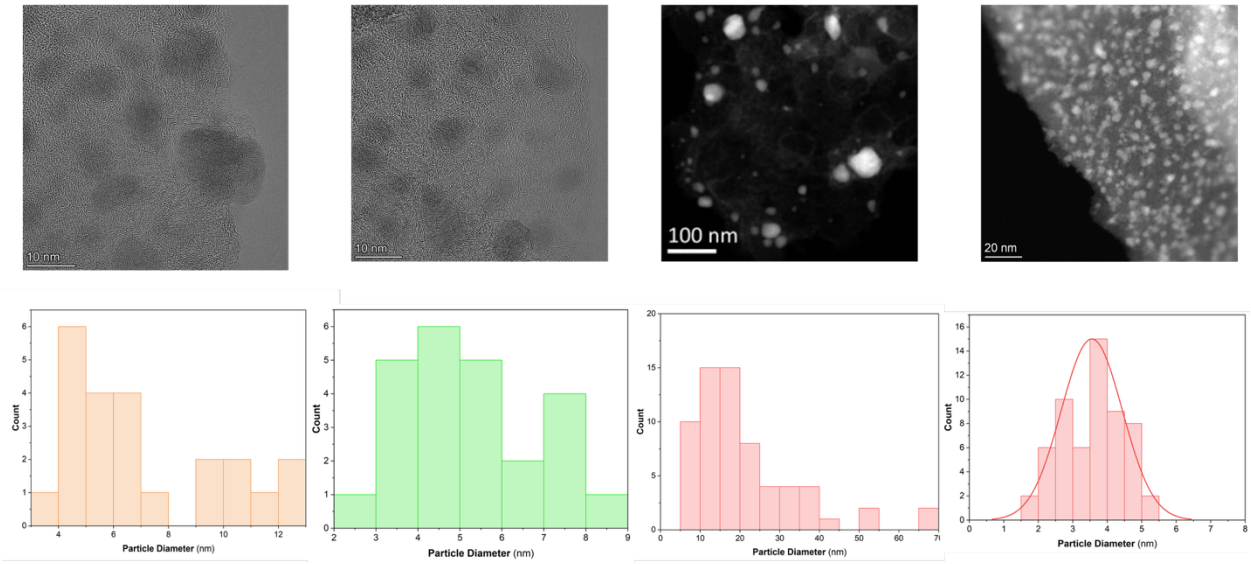

Figure S1. The Fe-Ni nanoparticle size distribution was obtained by analyzing multiple particles across several HAADF-STEM and HRTEM images. Particle sizes were measured using ImageJ software.

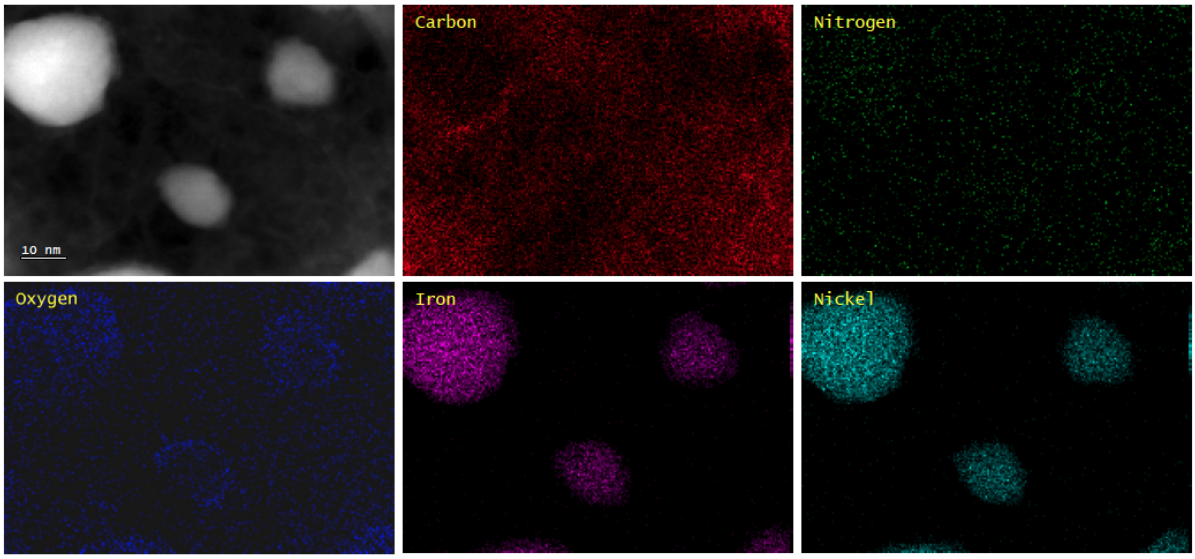

Figure S2. STEM-EDS analysis of the Fe-Ni nanoparticles revealed the presence of an oxide shell surrounding the metal cores.

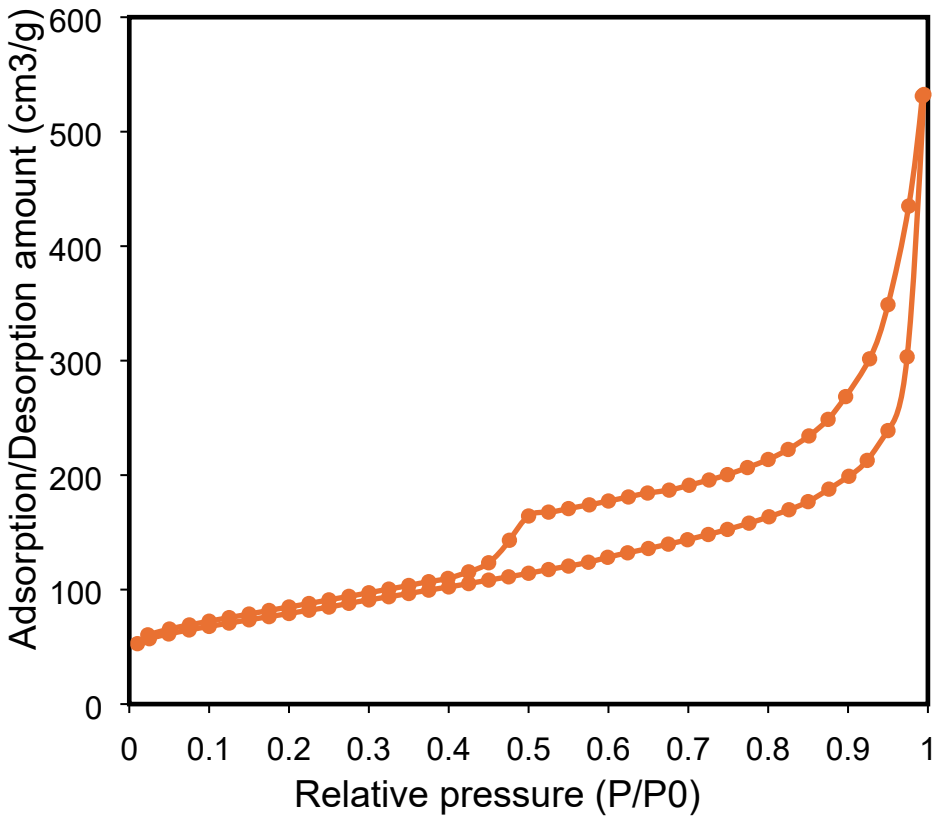

Figure S3. N_2 adsorption and desorption graph to analyze the surface area of the hierarchical Fe-Ni sample.

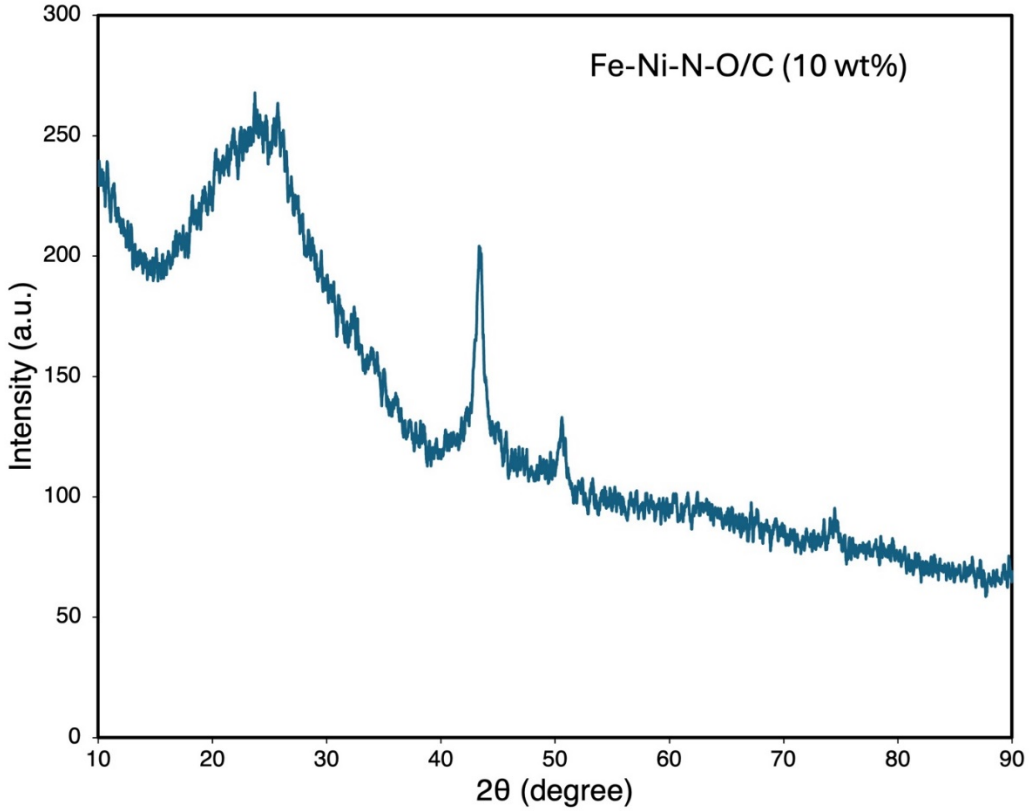

Figure S4. XRD pattern of Fe-Ni-N-O/C nanoparticles (10 wt%).

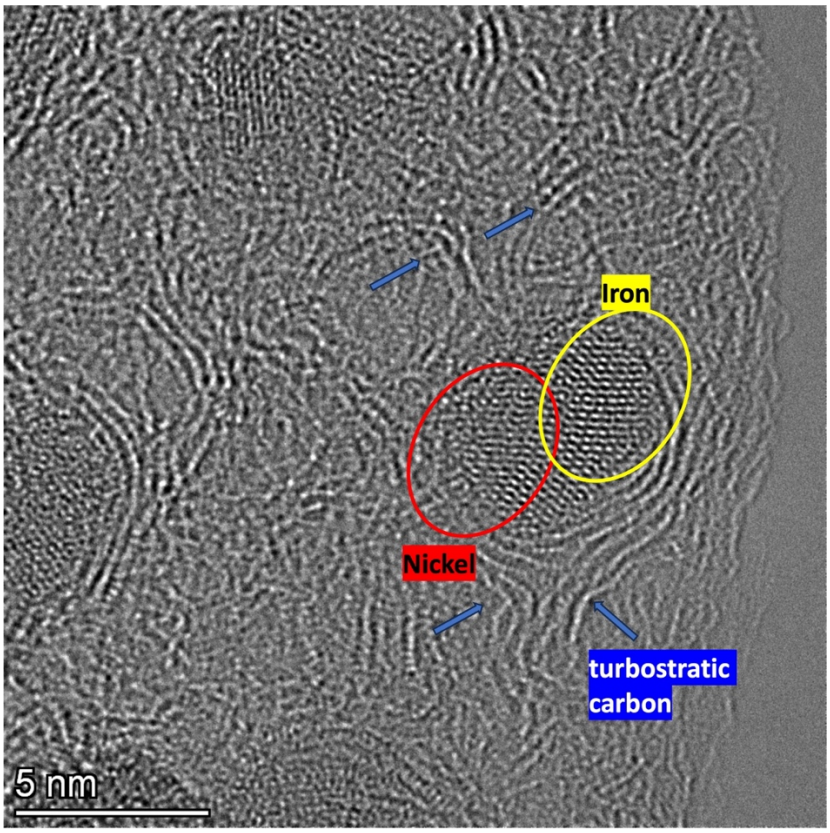

Figure S5. HRTEM image of small Fe-Ni-N-O/C nanoparticles (10 wt%)

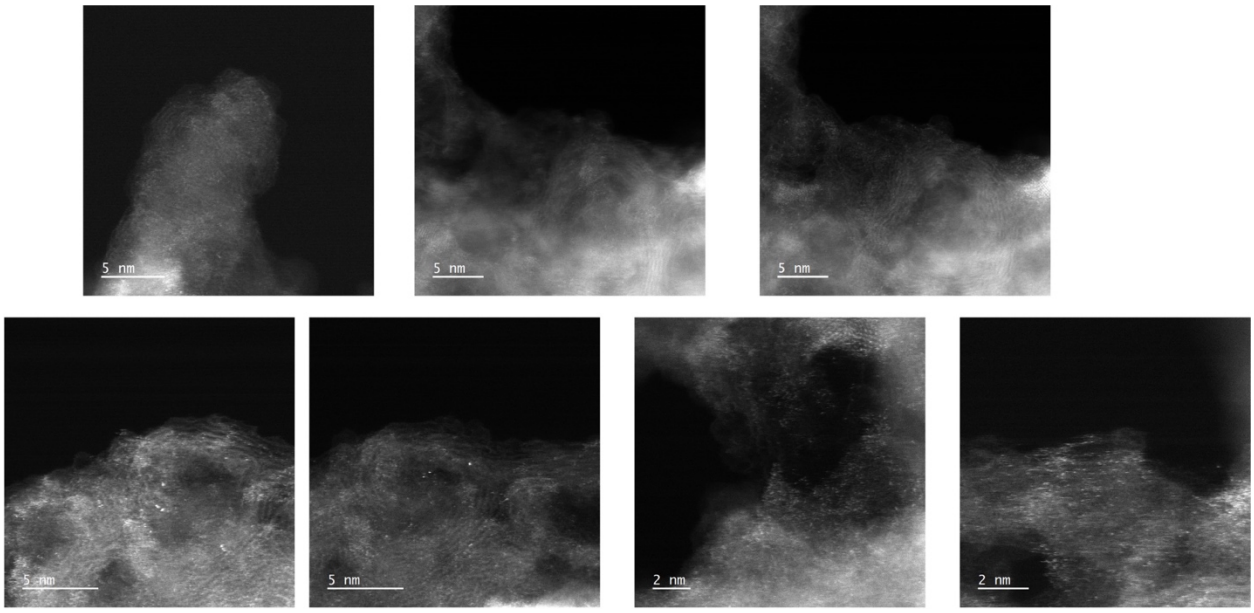

Figure S6. STEM images of Fe-Ni-N-O/C (10 wt%) samples in different areas to show the isolated Fe and Ni metal atom distribution.

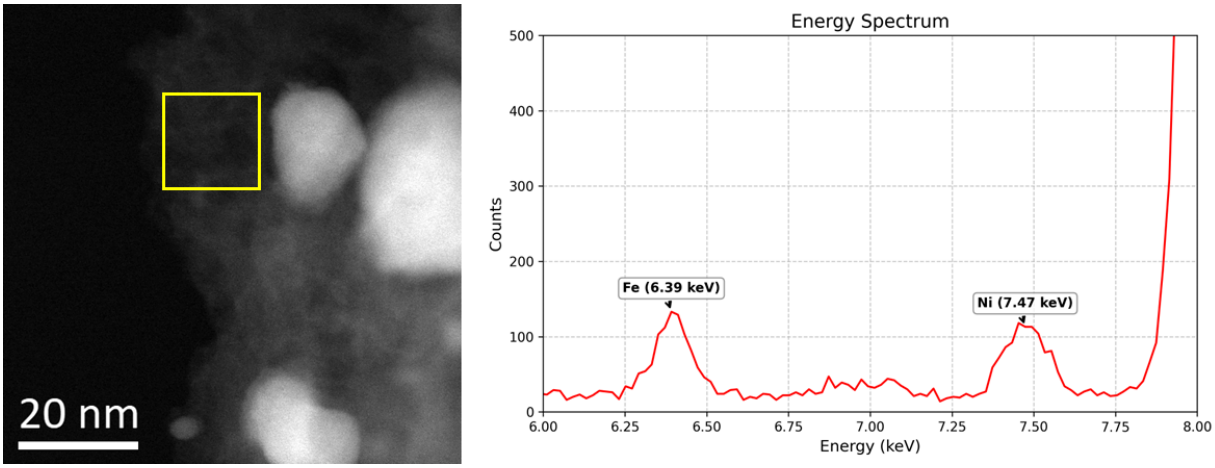

Figure S7. STEM image (Fe-Ni-N-O/C (10 wt%)) with EDS analysis from a region with no nanoparticles showing homogeneous Fe and Ni EDS signal from single atoms.

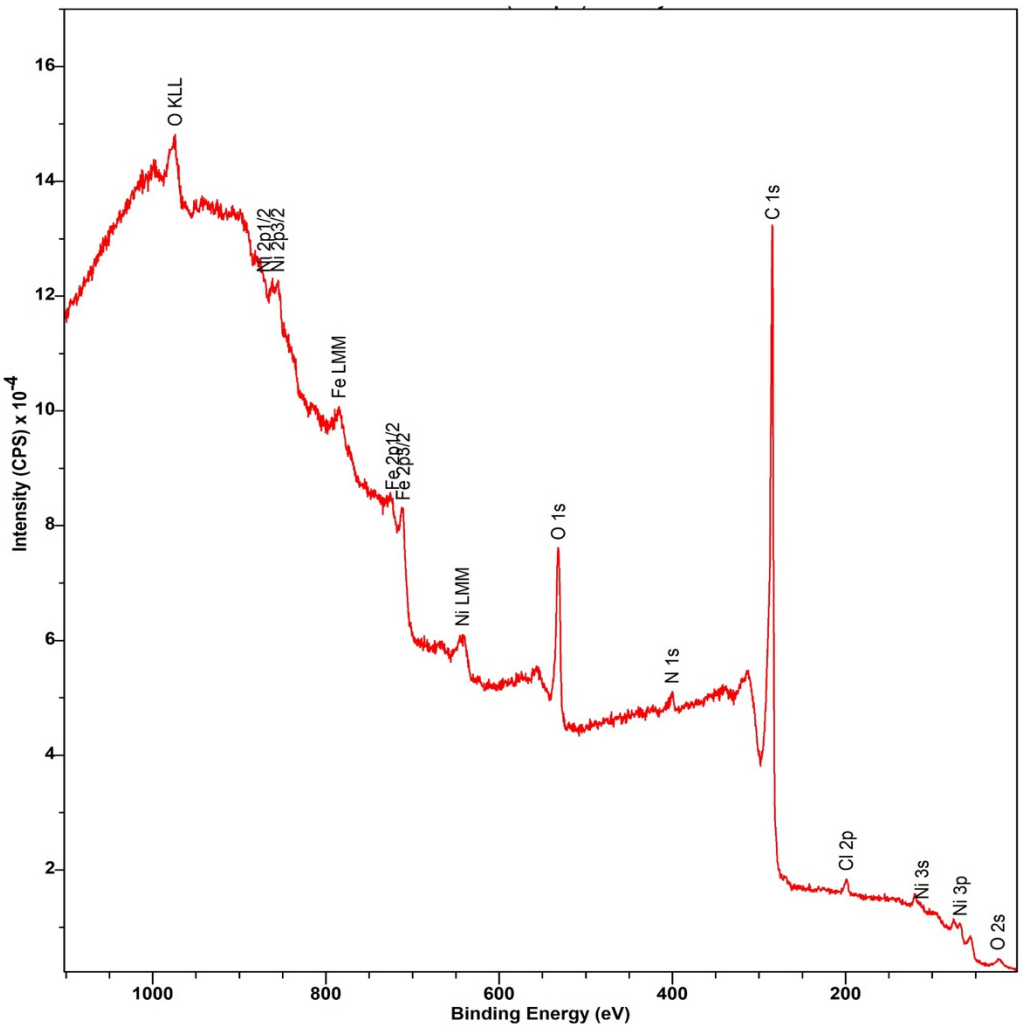

Sample (XPS)	C atomic %	Fe atomic %	N atomic %	Ni atomic %	O atomic %
Fe-Ni-N-O-C (metal loading 10 wt%)	90.7	2.0	2.1	1.8	3.4

Figure S7. XPS survey spectrum of Fe-Ni-N-C (10 wt%)

Figure S8. X-ray absorption spectroscopy (XAS) was performed at the Fe K-edge and Ni K-edge for Fe-Ni-N-C, Fe-N-C, and Ni-N-C catalysts (each containing 10 wt% metal). Various reference materials were used for comparison.

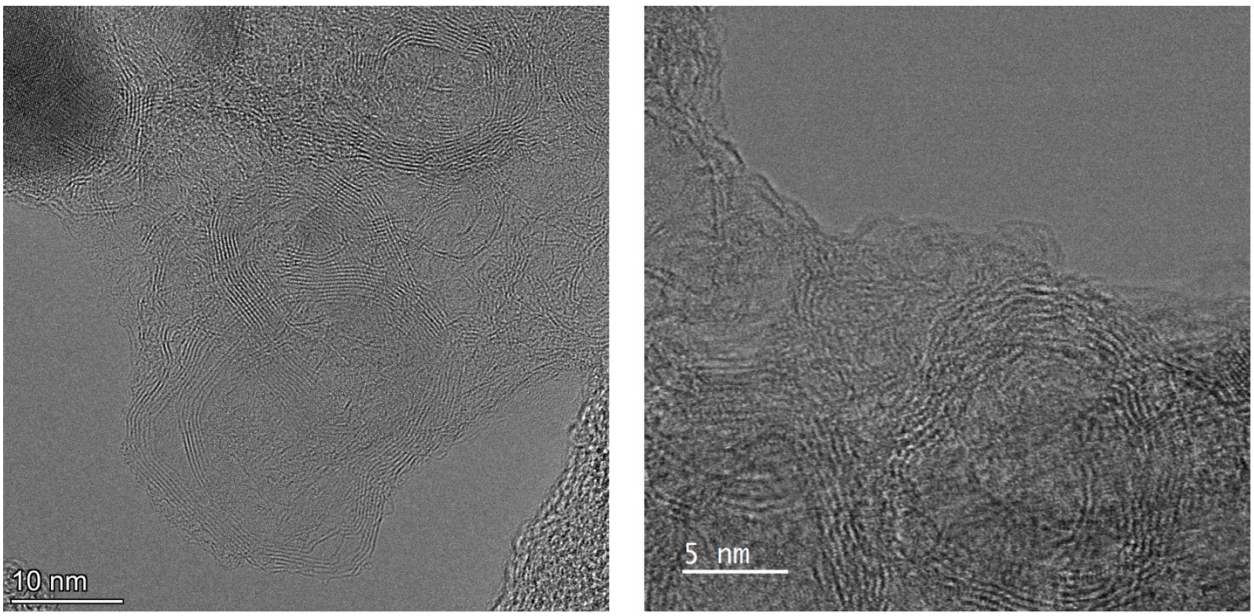

Figure S9. HRTEM image of turbostratic carbon for Fe-Ni-N-C (10 wt%)

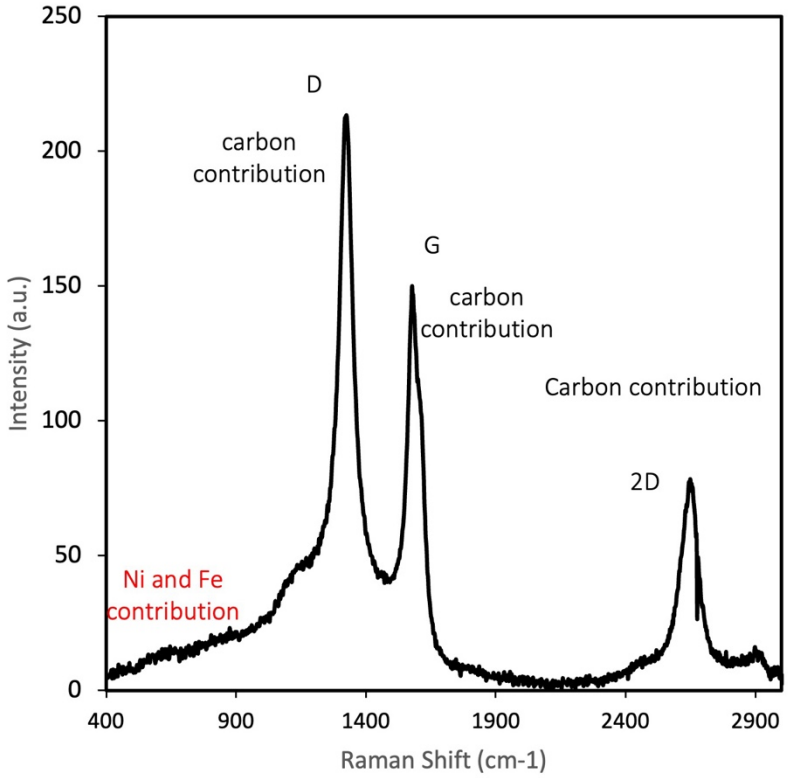

Figure S10. Raman spectrum of Fe-Ni-N-C (10 wt%). The 633 nm wavelength laser was used.

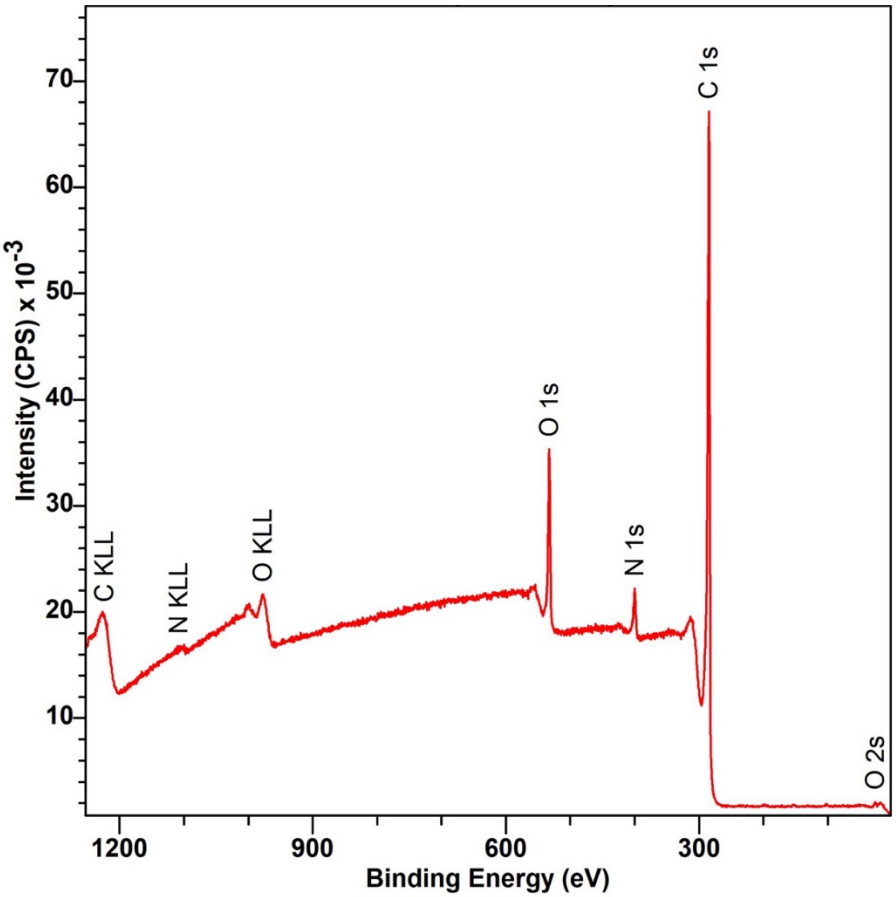

Sample	C	Fe/Ni	N	O
O-N/C	96.6	N/D	1.2	2.2

Figure S11. XPS survey spectrum of N-C (without any Fe and Ni).

Figure S12. High resolution XPS spectra of Cl 2p for Fe-Ni-N-O/C (10 wt%)

Figure S13. TEM images of (a) before and (b) after acid wash of 20 wt% Fe-Ni-N-C

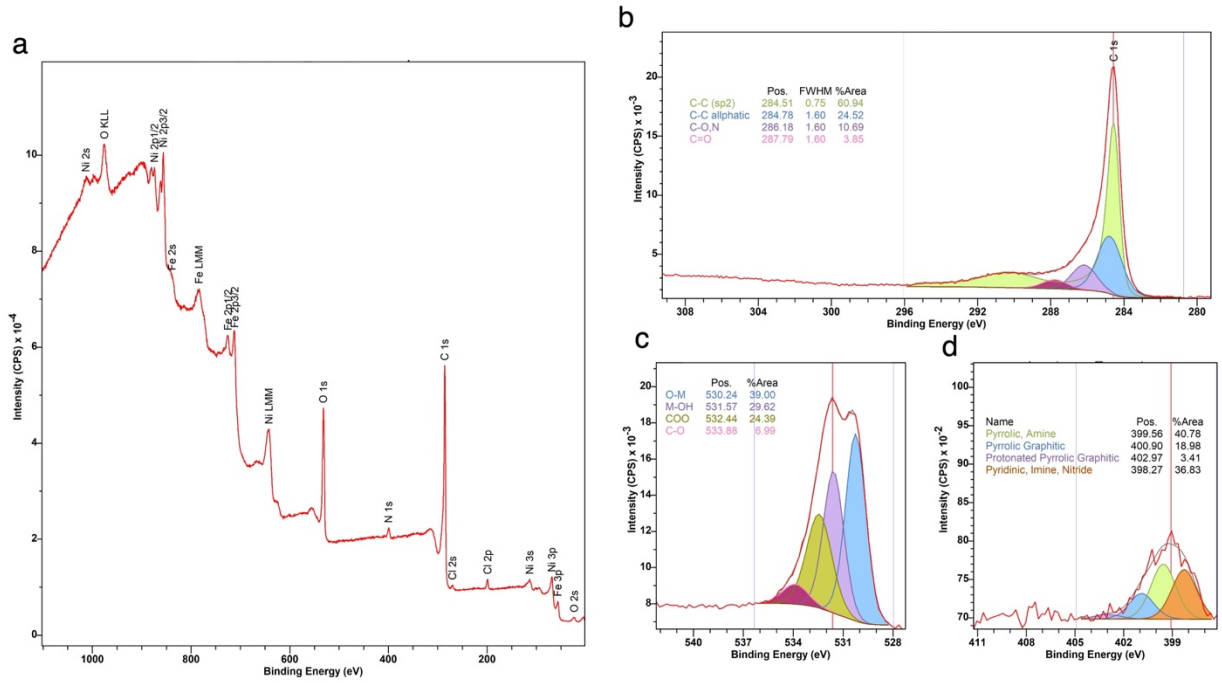

Figure S14. XPS spectra of Fe-Ni-N-C (20 wt%). (a) survey spectrum, (b) high-resolution C 1s, (c) high-resolution O 1s, and (d) high-resolution N 1s.

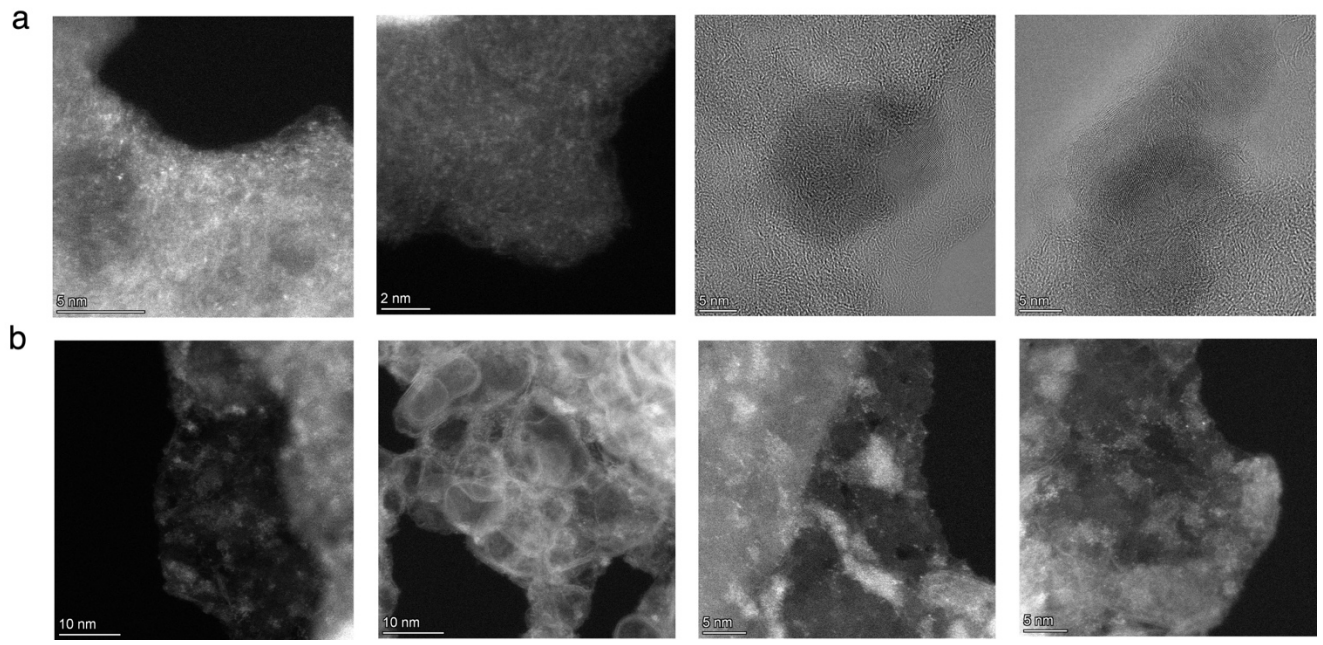

Figure S15. STEM and HRTEM images of (a) Ni-N-C (10 wt%) and (b) Fe-N-C (10 wt%) samples.

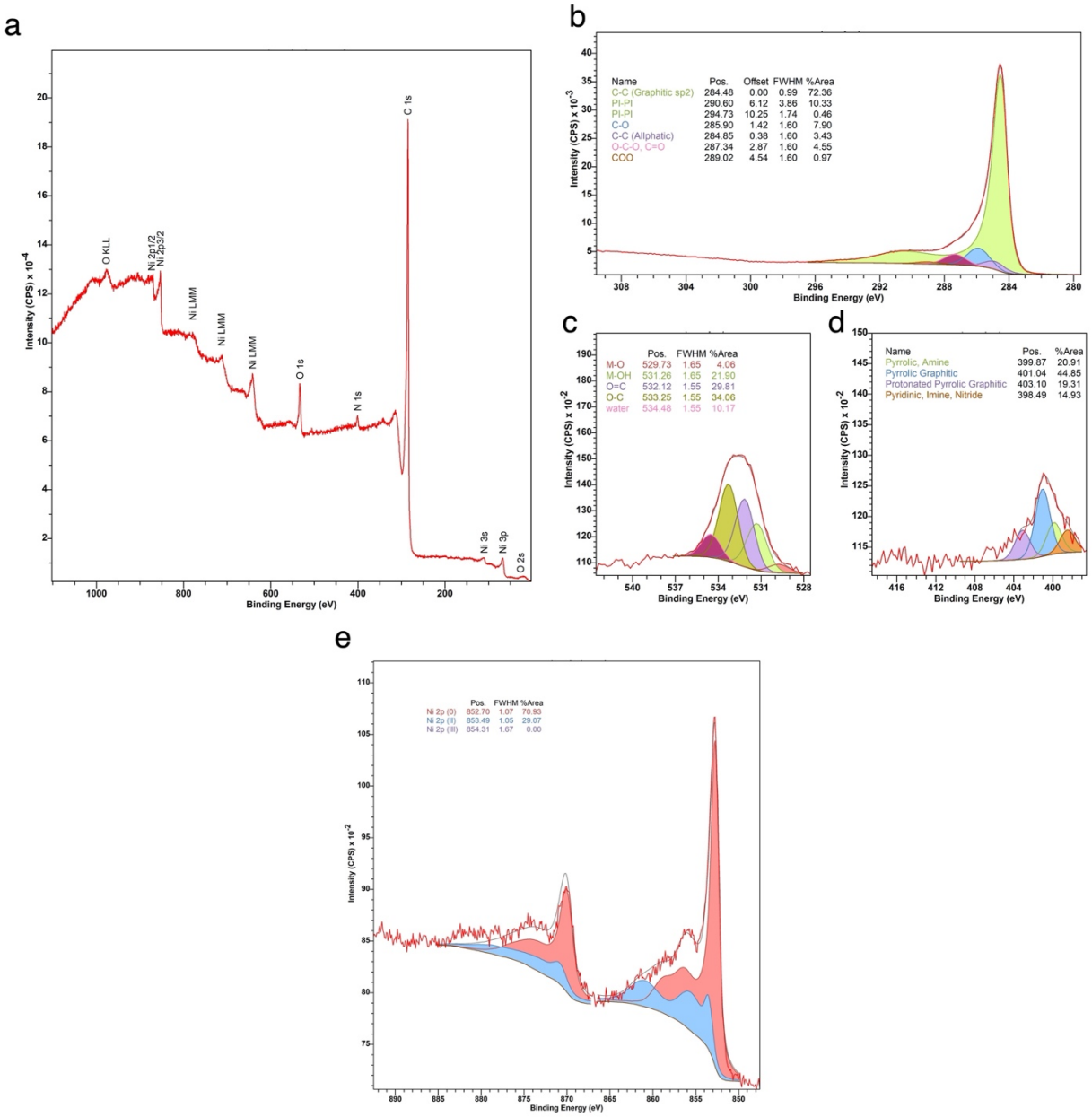

Figure S16. XPS spectra of Ni-N-C (10 wt%). (a) survey spectrum, (b) high-resolution C 1s, (c) high-resolution O 1s, (d) high-resolution N 1s, and (e) high-resolution Ni 2p.

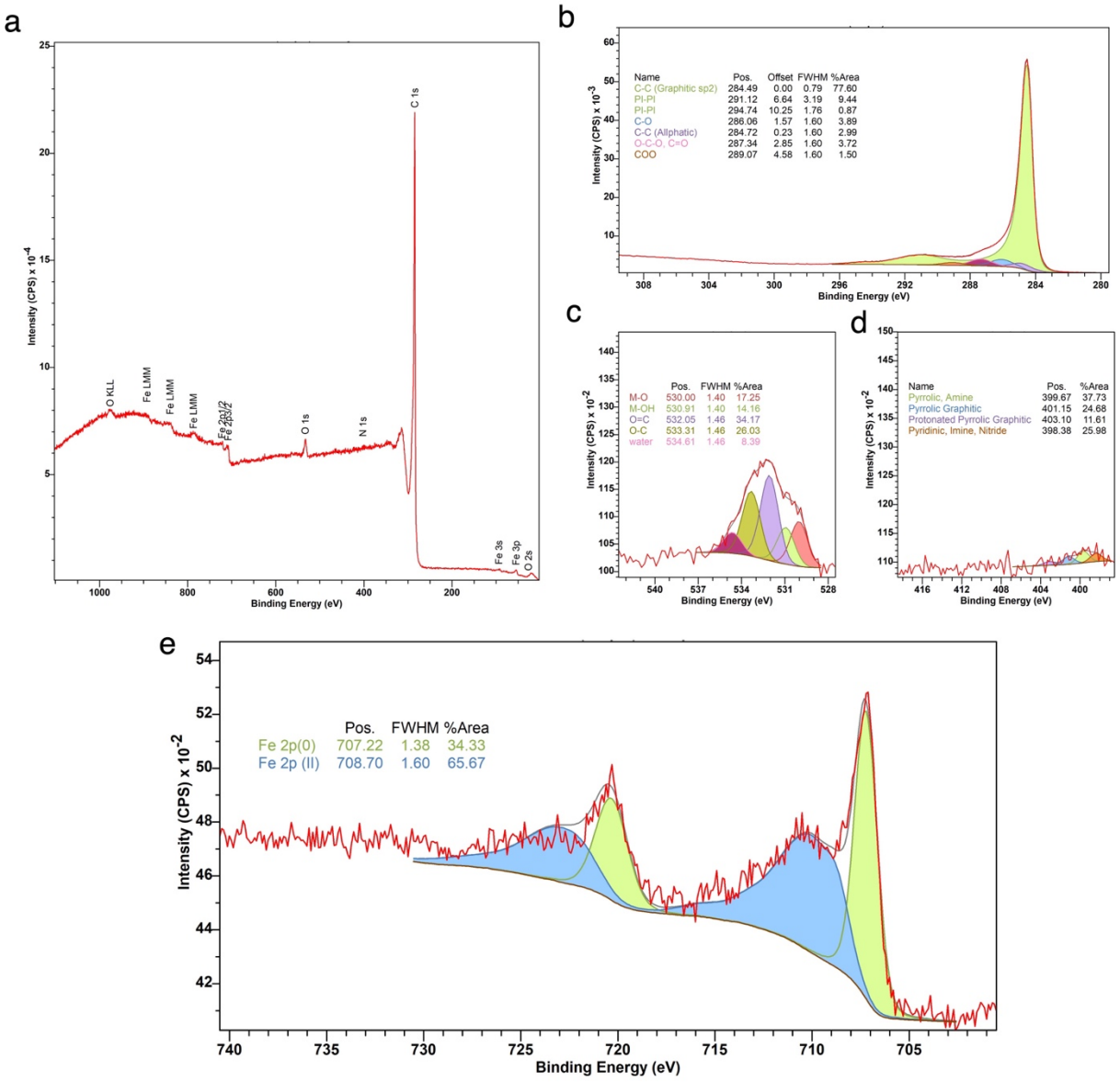

Figure S17. XPS spectra of Fe-N-C (10 wt%). (a) survey spectrum, (b) high-resolution C 1s, (c) high-resolution O 1s, (d) high-resolution N 1s, and (e) high-resolution Ni 2p.

Figure S18. CV activation curve (left) and Nyquist plots (right) of the Fe-Ni-N-C sample, showing a noticeable decrease in charge-transfer resistance with increasing potential.

Table S1. Comparison of various Fe-Ni and noble metal-based electrocatalysts at a current density of 10 mA/cm^2.

Electrocatalyst	Electrolyte	Overpotential at 10 mA/cm^2 (mV)	Tafel slope value at 10 mA/cm^2 (mV/decade)	References
Hierarchical Fe-Ni Nanostructures	**1M KOH**	**130**	**40**	**This work**
Conjugated phthalocyanine framework Fe/Ni	1M KOH	194	94	[1]
Ni–Fe oxide nanoparticles (8 nm)	1M KOH	290	58	[4]
S-doped Ni(Fe)OOH	1M KOH	198	17.5	[5]
iron–nickel dual atomic sites	1M KOH	294	67.4	[6]
Ni-$FeNi_3$/$Ni_{0.5-b}Fe_{0.5-y}Mo_{1.5}O_x$ nanohybrids	1M KOH	278	30	[7]
Phenalenyl-Based Dinuclear Ni(II) Complex	1M KOH	300	40	[8]
NiFeCuS	1M KOH	241	82.5	[9]
Ir-Doped Core–Shell Hollow Heterogeneous Nanospindles	1M KOH	217	62.1	[10]
Ru Nanoclusters	1M KOH	175	49	[11]
1D Monoclinic $Ir_xRu_{1-x}O_2$	0.5 M H_2So_4	180	50.3	[12]

Figure S19. (a) Mass activity, (b) ECSA-normalized activity, and (c) TOF of Fe-Ni-N-C are presented to evaluate its intrinsic catalytic performance.

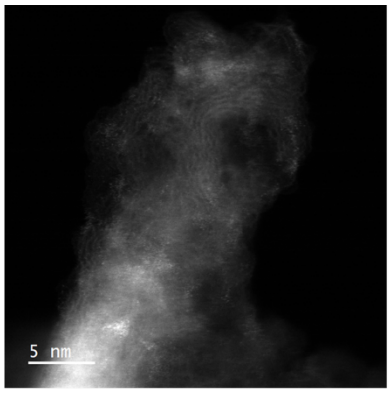

Potential (at 10 mA/cm^2) vs RHE	Tafel Slope Value
1.38 V	42 mV/decade

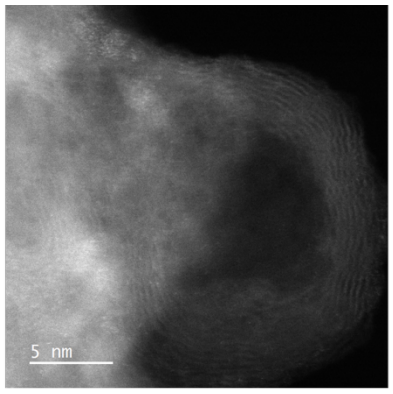

Potential (at 10 mA/cm^2) vs RHE	Tafel Slope Value
1.40 V	41.5 mV/decade

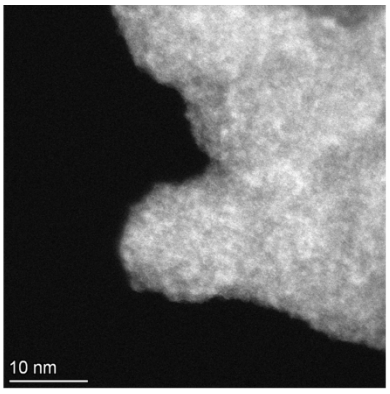

Potential (at 10 mA/cm^2) vs RHE	Tafel Slope Value
1.36 V	41.5 mV/decade

Figure S20. STEM images and corresponding electrochemical analyses by geometric surface area of independently synthesized Fe-Ni-N-C (10 wt%) batches.

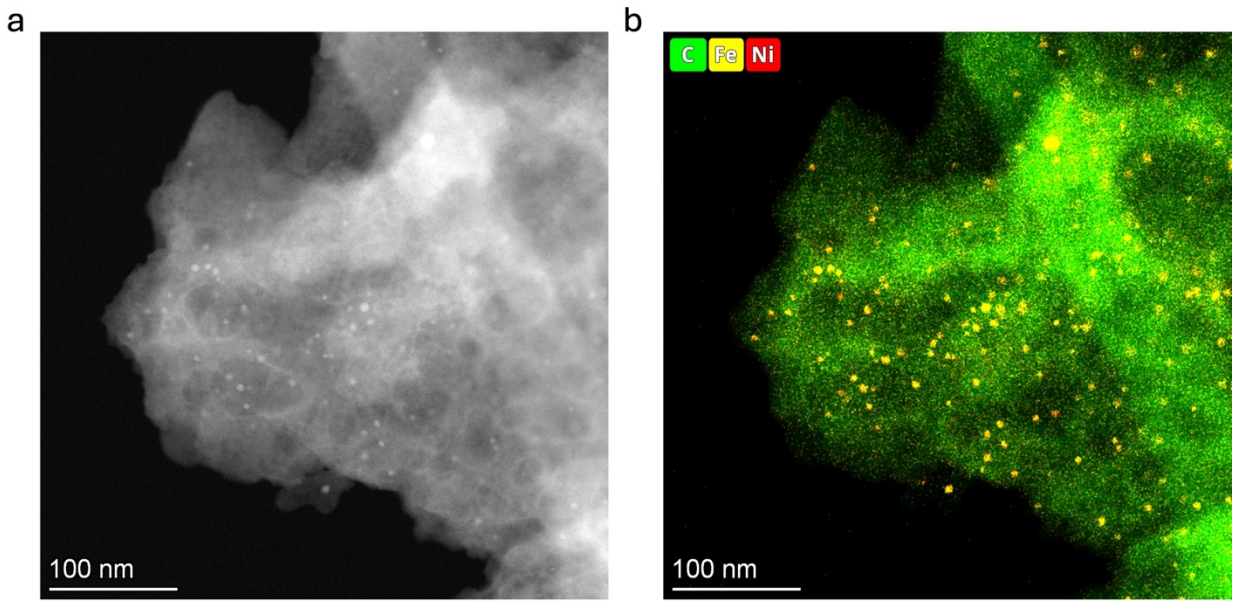

Figure S21. STEM and EDX images of the Fe-Ni-N-O/C (10 wt%) sample after 24 hours of acid washing in 2 M HCl.

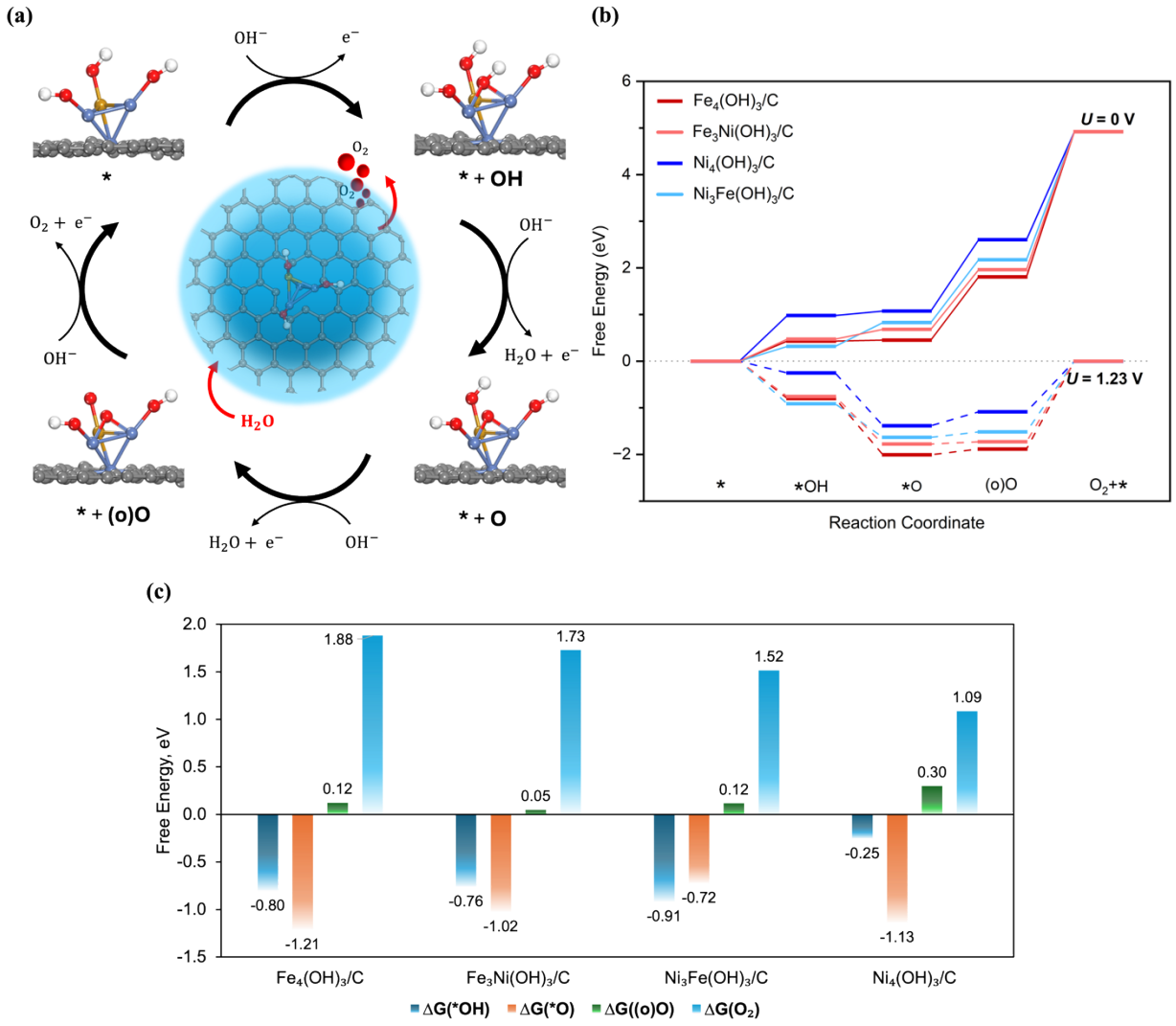

Figure S22: The OER reaction in alkaline media on hydroxylated metal clusters. (a) schematic representation of the OER mechanism on a Fe-doped Ni cluster model [$Ni_3Fe(OH)_3$/C], illustrating the four oxidation steps involving *, *OH, *O and (o)O species. The asterisk denotes the active site and (o) represents the oxidized cluster. Carbon, oxygen, hydrogen, nickel, and iron atoms are shown in gray, red, white, light purple, and brown, respectively; (b) free-energy diagram for the OER process at an applied potential of U_{RHE} = 0 V (solid line) and 1.23 V (dashed line); (c) comparison of free energies for individual OER steps for the different metallic clusters at an applied potential of U_{RHE} = 1.23 V.

Table S2. Hubbard U values (in V) for the (0001) facet of β-Fe/NiOOH determined by the linear response theory.

Composition	Ni	Fe
Ni_3Fe_1 - OOH	5.76	5.04
Ni_2Fe_2 - OOH	6.33	4.45
Ni_1Fe_3 - OOH	6.75	4.79
U_{avg}	6.28	4.76

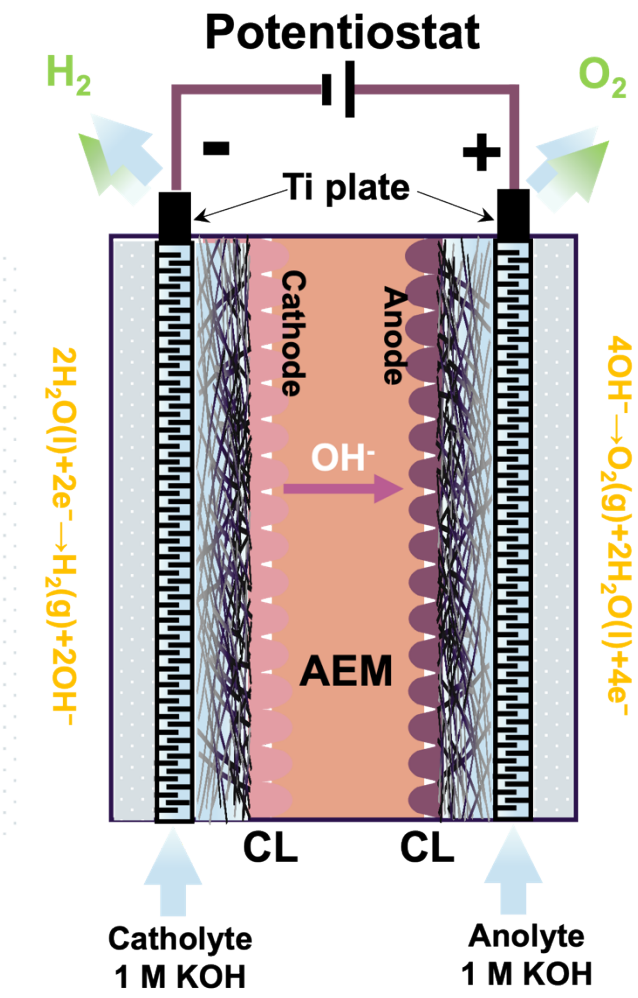

Figure S23. Schematic representation of a custom-made MEA water electrolysis cell

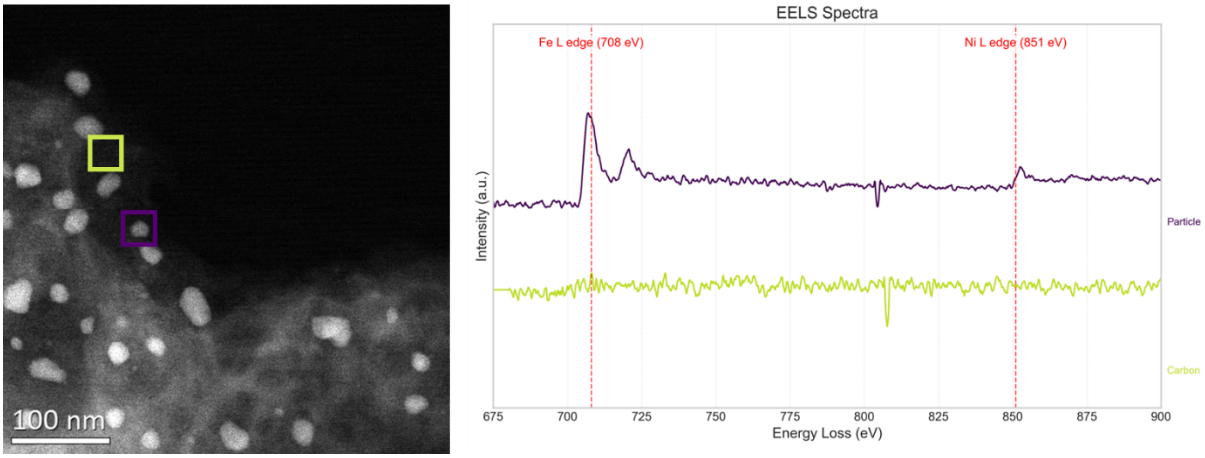

Figure S24. EELS spectra from two regions in the following the performance testing showing a lack of Fe and Ni in the carbon region, but no change in the Fe-Ni nanoparticles.

REFERENCES

1. Y. Zang, D.-Q. Lu, K. Wang, B. Li, P. Peng, Y.-Q. Lan and S.-Q. Zang, A pyrolysis-free Ni/Fe bimetallic electrocatalyst for overall water splitting, *Nature Communications*, 2023, **14**, 1792.
2. G. Kresse and J. Furthmüller, Efficiency of ab-initio total energy calculations for metals and semiconductors using a plane-wave basis set, *Computational Materials Science*, 1996, **6**, 15-50.
3. G. Kresse and J. Furthmüller, Efficient iterative schemes for ab initio total-energy calculations using a plane-wave basis set, *Physical Review B*, 1996, **54**, 11169-11186.
4. M. Yu, G. Moon, E. Bill and H. Tüysüz, Optimizing Ni–Fe Oxide Electrocatalysts for Oxygen Evolution Reaction by Using Hard Templating as a Toolbox, *ACS Applied Energy Materials*, 2019, **2**, 1199-1209.
5. Q. Li, B. Chen, L. Huang, S. Zhu, Y. Qian, D. Wu, S. Luo and A. Xie, S-doped Ni(Fe)OOH bifunctional electrocatalysts for overall water splitting, *International Journal of Hydrogen Energy*, 2024, **51**, 1392-1406.
6. L. Shan, Y. Liu, Y. Chen, X. Zhang, H. Dai, D. Xu, B. Yu, Y. Zhang, S. Chen, T. He and X. Ouyang, High-Density Iron–Nickel Dual Sites in Carbon Aerogels as Effective Alkaline Water/Seawater Oxidation Electrocatalysts, *ACS Sustainable Chemistry & Engineering*, 2025, **13**, 311-320.
7. J. Fan, X. Zhang, M. Han, X. Xiang, C. Guo, Y. Lin, N. Shi, D. Xu, Y. Lai and J. Bao, Amorphous Ni–Fe–Mo Oxides Coupled with Crystalline Metallic Domains for Enhanced Electrocatalytic Oxygen Evolution by Promoted Lattice-Oxygen Participation, *Small*, 2024, **20**, 2303927.
8. N. Kamboj and R. K. Metre, Designing a Phenalenyl-Based Dinuclear Ni(II) Complex: An Electrocatalyst with Two Single Ni Sites for the Oxygen Evolution Reaction (OER), *Inorganic Chemistry*, 2024, **63**, 9771-9785.
9. F. N. I. Sari, Y.-C. Lai, Y.-J. Huang, X.-Y. Wei, H. Pourzolfaghar, Y.-H. Chang, M. Ghufron, Y.-Y. Li, Y.-H. Su, O. Clemens and J.-M. Ting, Electronic Structure Engineering in NiFe Sulfide via A Third Metal Doping as Efficient Bifunctional OER/ORR Electrocatalyst for Rechargeable Zinc-Air Battery, *Advanced Functional Materials*, 2024, **34**, 2310181.
10. W. Liang, Y. Li, N. Zhang, J. Li, S. Li, Z. Wu and Y. Du, Ir-Doped Core–Shell Hollow Heterogeneous Nanospindles for Electrocatalytic Oxygen Evolution Reaction, *Inorganic Chemistry*, 2024, **63**, 14691-14698.
11. W. Chen, W. Wei, F. Li, Y. Wang, M. Liu, S. Dong, J. Cui, Y. Zhang, R. Wang, K. Ostrikov and S.-Q. Zang, Tunable Built-In Electric Field in Ru Nanoclusters-Based Electrocatalyst Boosts Water Splitting and Simulated Seawater Electrolysis, *Advanced Functional Materials*, 2024, **34**, 2310690.
12. K. Qin, H. Yu, W. Zhu, Y. Zhou, Z. Guo, Q. Shao, Y. Wu, X. Wang, Y. Li, Y. Ji, F. Liao, Y. Liu, Z. Kang and M. Shao, 1D Monoclinic IrxRu1-xO2 Solid Solution with Ru-Enhanced Electrocatalytic Activity for Acidic Oxygen Evolution Reaction, *Advanced Functional Materials*, **n/a**, 2402226.